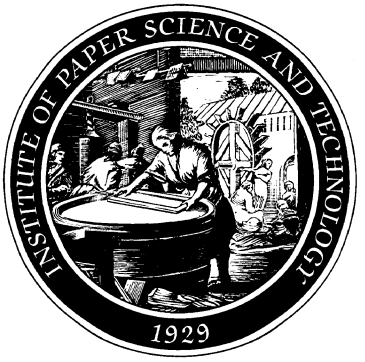

Institute of Paper Science and Technology
Atlanta, Georgia

IPST Technical Paper Series Number 858

Random Fiber Networks and Special Elastic Orthotropy of Paper

M. Ostoja-Starzewski and D.C. Stahl

June 2000

Submitted to
Journal of Elasticity

INSTITUTE OF PAPER SCIENCE AND TECHNOLOGY
PURPOSE AND MISSIONS

The Institute of Paper Science and Technology is an independent graduate school, research organization, and information center for science and technology mainly concerned with manufacture and uses of pulp, paper, paperboard, and other forest products and byproducts. Established in 1929 as the Institute of Paper Chemistry, the Institute provides research and information services to the wood, fiber, and allied industries in a unique partnership between education and business. The Institute is supported by 52 North American companies. The purpose of the Institute is fulfilled through four missions, which are:

- to provide a multidisciplinary graduate education to students who advance the science and technology of the industry and who rise into leadership positions within the industry;
- to conduct and foster research that creates knowledge to satisfy the technological needs of the industry;
- to provide the information, expertise, and interactive learning that enables customers to improve job knowledge and business performance;
- to aggressively seek out technological opportunities and facilitate the transfer and implementation of those technologies in collaboration with industry partners.

ACCREDITATION

The Institute of Paper Science and Technology is accredited by the Commission on Colleges of the Southern Association of Colleges and Schools to award the Master of Science and Doctor of Philosophy degrees.

NOTICE AND DISCLAIMER

The Institute of Paper Science and Technology (IPST) has provided a high standard of professional service and has put forth its best efforts within the time and funds available for this project. The information and conclusions are advisory and are intended only for internal use by any company who may receive this report. Each company must decide for itself the best approach to solving any problems it may have and how, or whether, this reported information should be considered in its approach.

IPST does not recommend particular products, procedures, materials, or service. These are included only in the interest of completeness within a laboratory context and budgetary constraint. Actual products, materials, and services used may differ and are peculiar to the operations of each company.

In no event shall IPST or its employees and agents have any obligation or liability for damages including, but not limited to, consequential damages arising out of or in connection with any company's use of or inability to use the reported information. IPST provides no warranty or guaranty of results.

RANDOM FIBER NETWORKS AND SPECIAL ELASTIC ORTHOTROPY OF PAPER

M. Ostoja-Starzewski

Institute of Paper Science and Technology
500 10th St., N.W., Atlanta, GA 30318-5794
e-mail: martin.ostoja@ipst.edu

and

D.C. Stahl

Architectural Engineering and Building Construction
Milwaukee School of Engineering
Milwaukee, WI 53202-3109
e-mail: stahl@msoe.edu

Shortened Title:
RANDOM NETWORKS AND SPECIAL ORTHOTROPY

1991 AMS Mathematics Subject Classifications:
70 Mechanics of particles and systems
73 Mechanics of solids
82 Statistical mechanics, structure of matter

Key Words:
random media, random fiber networks, special orthotropy, mechanics of paper, scale effects

Abstract

We consider a particular in-plane elastic orthotropy observed experimentally for various types of paper, namely: $S_{1111} + S_{2222} - 2S_{1122} = S_{1212}$, where S_{ijkl} are components of the in-plane compliance tensor. This is a statement of the invariance of in-plane shear compliance S_{1212}, which has been observed in some studies but questioned in others. We present a possible explanation of this "special orthotropy" of paper, using an analysis in which paper is modeled as a quasi-planar random microstructure of interacting fiber-beams - a model especially well suited for low basis weight papers. First, it is shown analytically that, without disorder a periodic fiber network fails the special orthotropy. Next, using a computational mechanics model, we demonstrate that two-scale geometric disorder in a fiber network is necessary to explain this orthotropy. Indeed, disordered networks with weak flocculation best satisfy this relationship. It is shown that no special angular distribution function of fibers is required, and that the uniform strain assumption should not be used. Finally, it follows from an analogy to the thermal conductivity problem that the kinematic boundary conditions, rather than the traction ones, lead quite rapidly to relatively scale-independent effective constitutive responses.

1. Introduction

This study was motivated by a peculiar aspect of in-plane elastic orthotropy of paper [1], and is an effort to use a fiber network model to reproduce and understand the behavior. The observation, apparently first reported by Horio and Onogi [2], is that Young's modulus at an arbitrary angle θ in the plane of a sheet, E_θ, is dependent only on Young's moduli in the principal material directions (1 and 2). The relation given in [2],

$$\frac{1}{E_\theta} = \frac{(\cos\theta)^2}{E_1} + \frac{(\sin\theta)^2}{E_2} \tag{1}$$

was observed by them to be a good predictor of experimental data for a wide variety of papers. This equation obviously differs from the relation derived from proper transformation of coordinates:

$$\frac{1}{E_\theta} = \frac{(\cos\theta)^4}{E_1} + \left(\frac{2\nu_{12}}{E_1} + \frac{1}{G_{12}}\right)(\cos\theta)^4 (\sin\theta)^4 + \frac{(\sin\theta)^4}{E_2} \tag{2}$$

Later, Campbell [3] showed that (1) is satisfied only if

$$\frac{1}{G_{12}} = \frac{1+\nu_{12}}{E_1} + \frac{1+\nu_{21}}{E_2} \tag{3}$$

and suggested that it is true for all papers. A third expression of the same behavior clearly illustrates the relationship between the in-plane compliances:

$$S_{1212} = S_{1111} + S_{2222} - 2S_{1122} \tag{4}$$

We shall use the term "special orthotropy" to describe the satisfaction of equations (1), (3), or (4).

Over the years, other researchers have reported mixed success in attempts to verify that paper elastic properties do indeed satisfy the requirements for special orthotropy. Craven and Taylor

[4] showed that for a variety of machine made kraft papers (1) is a very good predictor of E_θ. Jones [5] noted that one result of special orthotropy is that shear modulus is independent of orientation with respect to material principal directions, but his experimental data showed that G did vary with orientation. Jones demonstrated that (1) was a good predictor of Young's modulus at an angle, but he also noted that (2) was slightly better. Later, Suhling *et al.* [6] showed that (3) gave shear modulus within five percent of their careful experimental measurements.

This special relationship among the elastic properties is not observed in most materials - Liu and Ross [7] clearly showed that it is not true for wood. The question becomes, therefore, under what conditions can it occur in paper?

Schulgasser [8] tried to explain equation (4), using the so-called Cox model [9]. This model provides an analytical derivation of the in-plane compliance of a mat of infinitely long fibers, laid in a plane according to a Fourier series-type probability density function

$$p(\theta) = \frac{1}{\pi}(1 + a_1 cos2\theta + a_2 cos4\theta + \ldots + a_n cos2n\theta + \ldots) \qquad 0 < \theta \leq \pi \qquad (5)$$

In equation (5), θ is the angle a fiber makes with respect to the x-axis and it must be between zero and π. Note that the x and y-axes are referred to as the MD (machine) and CD (cross) directions, respectively, and paper is a disordered fiber system in the MD-CD plane with slight out-of-plane fiber orientation angles. The Cox model involves an assumption that all the fibers carry axial forces only, which necessarily implies that they interact via frictionless pivots. This, combined with the fact that they are infinite, results in the entire fiber network deforming by a uniform strain. The Cox model generally leads to good estimates of effective Young's moduli but

underestimates the shear modulus, both for isotropic and orthotropic systems. Schulgasser [8] showed that the Cox model results in (4) when (5) is used with

$$a_2 = \frac{(a_1)^2}{2} \qquad a_i = 0 \qquad i \geq 3 \tag{6}$$

or when a wrapped Cauchy distribution is used in place of (5):

$$f(\theta) = \frac{1}{\pi}\left(\frac{1-\rho^2}{1+\rho^2-2\rho\cos\theta}\right) \qquad 0 < \theta \leq \pi \qquad 0 \leq \rho \leq 1 \tag{7}$$

Finally, Schulgasser and Page [10] showed that a model of paper treated as a laminate composite could yield the special orthotropic relations as well, providing certain values of fiber moduli were used; this model, too, relied on the uniform strain assumption.

It must be kept in mind that, strictly speaking, the Cox model does not possess generic rigidity. This pathological behavior can be removed by the introduction of rigid fiber-fiber bonds (justified by the presence of hydrogen bonding between cellulose fibers) and fiber flexural stiffness. In other words, the fiber network should be modeled as a 2-D or 3-D frame of beam elements, and this is the starting point of the present study, partially communicated in [11]. In particular, we show that an analysis which simulates the heterogeneous three-dimensional network of fibers in paper, avoiding several of the assumptions that made the Cox model attractive for its simplicity, can reproduce the conditions of special orthotropy. In this computationally intensive procedure, fibers can transmit axial and shear forces and bending and torsional moments between rigid bonds. The present form of analysis is justified on three counts:

(i) Hydrogen bonds between fibers are not perfect hinges; mechanically we have a frame rather than a truss. Motivated by the experiments dating back to Page *et al.* [12], researchers have described paper fibers as carrying shear and moment in addition to axial loads [13]. In fact, it

was shown in the latter reference that the Cox model is not well-posed as it admits floppy (mechanism-type) modes of motion.

(ii) It is shown that triangular periodic beam networks can satisfy (4) only under a specific geometric condition (which renders them isotropic, so the point is moot), and so, disordered networks are necessary if we are to explore special orthotropy.

(iii) Once we have made the leap to analysis of disordered networks, it is not difficult to include important geometric features such as fiber flocs (clusters). We show that any disorder, especially non-uniform areal distribution of fibers into flocs, produces strain fields which are not uniform.

In the last Section we consider the issue of scale dependence of effective properties. A guidance in this respect is provided by the in-plane thermal conductivity of the fiber networks. Essential boundary conditions yield a conductivity tensor, while the natural ones yield a resistivity tensor. The ensemble averages of these two tensors lead to scale-dependent bounds on the macroscopic, effective conductivity; these bounds converge the more the network size approaches the classical continuum limit of a Representative Volume Element. While there is no one-to-one analogy between the in-plane conductivity and the in-plane elasticity, this study indicates that the essential boundary conditions lead, more rapidly than the natural ones, to relatively scale-independent effective constitutive responses.

2. Planar Periodic Fiber Networks

In Figure 1 we introduce a highly idealized, albeit exactly solvable, model of a network of fiber-beams, a triangular lattice specified by the angle α. For simplicity the lattice nodes are assumed to have the same thickness as a single fiber. Each fiber is taken to have a rectangular cross section of height t and width w, with the distance between nodes equal to s. Such a beam

lattice was analyzed by Wozniak [14] and also reported in his earlier papers, but given the presence of short fiber segments in the present case, we use the Timoshenko (rather than Bernoulli-Euler) beam model to admit beam shear deformation.

An equivalent in-plane continuum is a micropolar one (e.g., [15]), and therefore, the strain energy density in each unit cell (defined by hexagons in Figure 1) is given as:

$$U_{continuum} = \frac{1}{2}\gamma_{ij}C^{(1)}_{ijkm}\gamma_{km} + \frac{1}{2}\kappa_{i3}C^{(2)}_{i3k3}\kappa_{k3} \tag{8}$$

where γ_{ij} is a (generally asymmetric) strain tensor and κ_{i3} is the torsion-bending tensor. Conjugate to these are the (generally asymmetric) force-stresses τ_{ij}, and moment-stresses μ_{i3}, $i, j = 1, 2$. The in-plane stiffness tensors $C^{(1)}_{ijkl}$ and $C^{(2)}_{i3k3}$ are found as

$$C^{(1)}_{ijkm} = \sum_{b=1}^{6} n_i^{(b)} n_k^{(b)} (n_j^{(b)} n_m^{(b)} R^{(b)} + \tilde{n}_j^{(b)} \tilde{n}_m^{(b)} \tilde{R}^{(b)}) \qquad C^{(2)}_{i3k3} = \sum_{b=1}^{6} n_i^{(b)} n_k^{(b)} S^{(b)} \tag{9}$$

where $n^{(b)}$ and $\tilde{n}^{(b)}$ are components of the unit vectors along and normal to a fiber b, and

$$R^{(b)} = \frac{2EA}{s\sqrt{3}} \qquad \tilde{R}^{(b)} = \frac{24EI}{(1+\beta)s^3\sqrt{3}} \qquad S^{(b)} = \frac{2EI}{s\sqrt{3}} \tag{10}$$

In (10) E, A, and I are the fiber modulus of elasticity, cross sectional area, and moment of inertia. As noted earlier, s is the lattice spacing. In (9) it is assumed that all fibers are identical. Also,

$$\beta = \frac{12EI}{GAs^2} = \frac{E}{G}\left(\frac{w}{s}\right)^2 \tag{11}$$

is the dimensionless ratio of bending to shear stiffness of Timoshenko beams.

In order to check the special orthotropy relation, we need to determine a shear compliance in the classical sense. We do this by imposing the strain tensor's symmetry, i.e., by setting

$\gamma_{12} = \gamma_{21} = \varepsilon_{12}$ (classical shear strain), whereupon we find two shear moduli G_{12} and G_{21} in the classical (non-micropolar) relations

$$\tau_{12} = 2G_{12}\gamma_{12} = (C^{(1)}_{1212} + C^{(1)}_{1221})\gamma_{12} \qquad \tau_{21} = 2G_{21}\gamma_{12} = (C^{(1)}_{2121} + C^{(1)}_{2112})\gamma_{12} \quad (12)$$

In fact, G_{12} and G_{21} turn out to be equal, so that we simply have G. Thus, also the force-stress becomes symmetric $\tau_{12} = \tau_{21}$, which is then identified with the classical Cauchy stress σ_{12}.

Working with $(9)_1$, (10), and (12) for a periodic network of Figure 1 made of identical fibers ($R^{(b)} = R$, etc.), and with the orientation angle α as a free parameter, we find the following expressions for compliance terms of interest to us

$$\begin{aligned}
S_{1111} &= \frac{-R + (\cos\alpha)^2(R - \tilde{R})}{R(-R + \cos\alpha^2(R - 3\tilde{R}))} \\
S_{2222} &= \frac{R + 2(\cos\alpha)^4(R - \tilde{R}) + 2(\cos\alpha)^2\tilde{R}}{2R(R - (\cos\alpha)^2(2R - 3\tilde{R}) + (\cos\alpha)^4(R - 3\tilde{R}))} \\
S_{1122} &= S_{2211} = \frac{(\cos\alpha)^2(R - \tilde{R})}{R(-R + (\cos\alpha)^2(R - 3\tilde{R}))} \\
S_{1212} &= \frac{2}{-\tilde{R} + 2(\cos\alpha)^2(2R - \tilde{R}) + (\cos\alpha)^4(R - \tilde{R})}
\end{aligned} \quad (13)$$

These can satisfy the special orthotropy condition (4) for angle $\alpha = 60^o$ only (i.e., equilateral triangular lattice), which creates an *isotropic* network so the point is moot.

On the other hand, if we keep $\alpha = 60^o$ but work with three different fibers types at angles 0^o, 60^o, and 120^o, respectively, we get an anisotropic network that violates (4).

There are two more (nearest-neighbor) periodic networks in two dimensions: square and hexagon. However, given their total inadequacy to model paper microstructure, we must discard

them although their lack of special orthotropy can also be demonstrated by a procedure analogous to that outlined above. All this leads us to a question: if we cannot devise a periodic fiber network that satisfies the special orthotropy conditions, can we satisfy those conditions with a network of random geometry?

3. Modeling and Computational Mechanics of Random Fiber Networks

3.1 Random geometry model

As is commonly done in mechanics of random media (e.g., [16]), the random fiber network $\boldsymbol{B}$ is taken as an ensemble $\{B(\omega);\omega \in \Omega\}$ with each body, or realization, $B(\omega)$ having a disordered geometry. We will now focus on finite-sized realizations in windows of size $L_x \times L_y \times t$ in the x,y,x coordinate system. L_x, L_y and t are the two in-plane dimensions and the z-thickness of paper, respectively. Upon introducing a dimensionless scale parameter $\delta = L/\langle l \rangle$, where $L = L_x = L_y$ and $\langle l \rangle$ is the average fiber length, we shall index the ensemble and its realizations by δ, so that $\boldsymbol{B}_\delta = \{B_\delta(\omega)\,;\, \omega \in \Omega\}$.

For a chosen δ, each $B_\delta(\omega)$ is generated in a box $L_x \times L_y \times t$ according to a germ-grain model (see [17] for general background and [29] for applications in micromechanics) so as to obtain fiber flocculation, commonly seen as grayscale effects in a typical sheet of paper held against light. This model is introduced constructively: we start with a point process $\Phi = \{\phi_1, \phi_2, \ldots\}$, that is spatially homogeneous in the x, y, z-space. The points ϕ_i are called germs. Next, on each ϕ_i we place a so-called grain Ξ_i, such that $\Xi_1, \Xi_2, \ldots$ form a sequence of independent, identically distributed random compact sets in the x, y, z-space, that are

independent of the Φ process. The germ-grain model is the union Ξ of the grains Ξ_i, translated by the ϕ_i in Φ

$$\Xi = \bigcup_{\phi_i \in \Phi} (\Xi_i + \phi_i) \tag{15}$$

Our grains Ξ_i are flocs of fibers, whereby each fiber's center is at a position $r = (r_x, r_y)$ relative to the floc's center, the floc being ϕ_i. In order to avoid arbitrarily close placement (i.e., near overalp) of flocs, we take Φ to be a hard-core process, i.e. one in which the minumum distance between any two ϕ_i's is non-zero. The unrealistic situations of near overlap of flocs would occur if Φ were taken as a Poisson point process, which would then result in Ξ being simply a Boolean model.

By using a random variable r_0 governed by the one-parameter triangular probability density function

$$p(r_0) = -\frac{b^2}{2} r_0 + b \qquad r_0 \in \left[0, \frac{2}{b}\right] \tag{16}$$

we generate coordinates for the location of a fiber center relative to the floc center

$$r_x = (1 + a_1) r_0 \cos\theta \qquad r_y = r_0 \sin\theta \tag{17}$$

where θ is the fiber's in-plane orientation angle controlled via (5) and a_1 is a parameter from (5). Function (16) is chosen so as to obtain clustering in a finite disk of radius $2/b$ if $a_1 = 0$, or in an ellipse if $a_1 > 0$. In the latter case the flocs are stretched in the machine direction according to the degree of preferred orientation of fibers so as to reflect typical structure of machine made paper. Note that as b increases, fibers are clustered into tight flocs of radius tending to zero as

$b \to \infty$, and as b decreases they are scattered - this is apparent in Figure 4 (left column). Equations (16-17) are simply a useful model to qualitatively obtain flucculation (clustering) effects; they are presently undergoing testing based on image anlysis of real papers.

We define the density d of the network as the total fiber length per unit MD-CD area. Coverage (average number of fibers per point) and sheet basis weight (weight per unit area) are obviously directly proportional to d. For a chosen d, a number of fibers to be assigned to the test volume is computed, and then each fiber is assigned at random, uniformly, to any of the germs. The fiber centers within each floc are not generated in a common z-plane; the z-coordinate is sampled from a uniform 'depth density'.

By keeping d and t independent, we can simulate papers with the same coverage but different degrees of compaction, corresponding to different degrees of pressing during papermaking. The degree of compaction is measured by the relative bonded area *RBA* defined as

$$RBA = \frac{A_{bonds}}{A_{projected}} \tag{18}$$

where A_{bonds} is the total area of all bond parallelograms, while $A_{projected}$ is the total projected area of all fibers (e.g., [18]).

This methodology reflects our understanding that the fiber network model is likely to be realistic only for papers that have relatively low *RBA*, so their primary load-carrying mechanism is transfer of forces and moments along fiber axes between nodes, rather than more complex interaction of plate- or solid-like fiber segments.

3.2 Mechanics model

Our computational mechanics model of fiber networks is based on the following assumptions

and steps (see also [19], [20]):

(i) Generate a system $B(\omega)$ of finite-length straight fibers according to the germ-grain model and the probability density functions controlling the spatial distribution of fibers and distribution of fiber orientations. The fibers are placed in three dimensions with possible non-zero angles to control out-of-plane orientation of the fiber axis and the "roll" of the fiber about its own axis.

(ii) Fibers may have different dimensions and mechanical properties, sampled from any prescribed statistical distribution.

(iii) Bonds are identified where the prismatic volumes of two fibers intersect. Bonds are rigid, but because fiber elements extend to the center of a bond, the end of the fiber element in what really is a bonded zone with finite dimension offers some simulation of bond flexibility.

(iv) Each fiber is a series of linear elastic three-dimensional Timoshenko beam elements e, with torsion included, between bonds with other fibers. This model has the capability to handle displacements and forces in three dimensions, but, in order to grasp scales several times larger than the floc size, we have disabled the out-of-plane degrees of freedom at each node. Thus, while the deformations are planar, the network geometry remains truly three-dimensional.

(v) Analysis of each and every $B(\omega)$ follows the laws of deterministic mechanics. In particular, having solved for the displacements and rotations of all the bonds under uniform kinematic boundary conditions $u_i = \varepsilon^0_{ij} x_j$, we establish the network's effective stiffness tensor

$C_{ijkm}(\omega)$ from a postulate of equivalence of the total strain energy of all the network's elements e, U_{tot}, with that of an effective continuum

$$\frac{V}{2}\varepsilon^0_{ij}C_{ijkm}(\omega)\varepsilon^0_{ij} = \sum_{e \in E}[U_e^{axial} + U_e^{shear} + U_e^{moment} + U_e^{torsion}] \qquad V = L_x L_y t \qquad (19)$$

The set $\{C_{ijkm}(\omega);\omega \in \Omega\}$ describes $\boldsymbol{B}$ in the ensemble sense. The $C_{ijkm}(\omega)$'s are, in fact, dependent on the window size. This dependence vanishes in the limit of infinitely large windows, which corresponds to the classical Representative Volume Element (RVE) in the sense of Hill [21]. It is argued in Section 6 that, in the case of random fiber networks - which, in fact, are a special type of porous materials [22] - the kinematic boundary condition allows a much faster asymptotic approach to the RVE than the uniform traction boundary condition $t_i = \sigma^0_{ji}n_j$. This homogenization concept much more closely grasps the real microstructure than various periodic or phenomenological models (e.g., [23]).

Finally we note that the present model also provides a stage for a progressive failure analysis, in which a prescribed displacement at one or more window edges is incremented and fiber and/or bond failures are serially identified due to the ongoing stress field redistribution. This analysis will not be discussed further in the present paper.

4. Analysis Results: Special Orthotropy

Network analysis was used to explore the relationship between variables controlling network geometry and the idea of special orthotropy. The variables considered were network thickness t, floc parameter b, and fiber orientation with the parameters a_i in (5). As noted earlier, changing t for a given coverage affects the network's *RBA*. All networks were 4 *mm* square, with 35 *mm* of

fiber per mm^2 area. All fibers were 1 *mm* long, 0.05 mm wide, and 0.015 *mm* thick. The resulting coverage is approximately 1.75.

Prior to discussing this data directly, we show some of the differences between the predictions of the present model and the Cox model. Example networks with each of five thicknesses and each of two degrees of scatter were analyzed. The networks were nominally isotropic, with all a_i of (5) equal to zero. Results shown in Figure 2 are the ratio of network modulus from the present analysis to the predictions of the Cox model applied to these geometries. Each data point shown represents the mean modulus for ten example networks; variability was low with standard deviations between 3 and 8 percent of means. The data show that the present model is 'softer' than the Cox model, as one should expect due to the present model's short fibers. The softness increases as thickness increases, because the networks become less well-connected (*RBA* decreases). Also, networks with tighter flocs are softer, as the sparse areas between flocs present little resistance to deformation.

Anisotropic networks were analyzed to evaluate special orthotropy. Two degrees of anisotropy were evaluated; some networks had a_1 of (5) equal to 0.5 and other a_i equal to zero, and some had a_1 equal to 0.5 and a_2 equal to 0.05. Closeness of fit to the condition of special orthotropy is given by a non-dimensional parameter we call the "Campbell number" (recall (4))

$$n_C \equiv \frac{S_{1111} + S_{2222} - 2S_{1122} - S_{1212}}{S_{1111} + S_{2222}} \tag{20}$$

Each point in Figure 3 represents the mean value for four example networks. The variability is high enough that we cannot make significant conclusions regarding the trends as network thickness increases, but we can make qualitative observations regarding the effect of flocculation

and fiber orientation. The data show that networks with little flocculation (low parameter b) can come closer to satisfying the Campbell relation than networks with tighter flocs (compare solid triangles and squares, or outlined triangles and squares). Also, networks with slightly less orientation (a_1 and a_2 nonzero) come closer to satisfying the Campbell relation than strongly oriented networks (compare solid and outlined shapes).

5. Analysis Results: Non-uniformity of Displacement Fields

Having made the argument that disorder plays a central role in establishing the relationships between the effective elastic properties, we now consider the effect of disorder on the uniformity of the displacement field. As a starting point we have the assumption inherent in closed-form solutions such as the Cox model, and in most mesoscale or cellular models, that the displacement of any point within the network is determined by a uniform strain field. Under this scenario, measures of non-uniformity such as, for example, the fiber's proximity to a floc do not affect its deformation. Clearly this assumption is appropriate for homogeneous materials.

To evaluate the effect of disordered network geometry on displacement fields, a series of networks with three degrees of flocculation was analyzed. Example networks are shown in the left column of Figure 4; they are 4 *mm* square with 30 *mm* of fiber length per square *mm* of the paper's in-plane area. The fibers are 0.05 *mm* wide, and this combined with the total fiber length gives a coverage of 1.5. Using a typical value for fiber coarseness, this is equivalent to approximately 8 $gram/m^2$ basis weight. The sheet thickness was 0.03 *mm*, and the resulting *RBA* varied from 0.56 to 0.66. There is no preferred direction in these networks - all coefficients in (5) are zero. The only parameter that was varied was the floc parameter, with the three values shown in Figure 4; in each case the germs (floc centers) were identical.

The networks were analyzed subject to a prescribed ε_{11}^{0}-strain on the boundaries. The figures in the right column of Figure 4 show the difference between the resulting displacement of each node and what the displacements would be if the strain field in the interior of the network had been uniform. If the displacement field had actually been uniform, the figures would consist simply of dots; the lines represent deviation from uniformity. Two qualitative observations can be made. First, the deviation from uniform displacements is certainly apparent in all three networks, even the one with low degree of flocculation. Second, there seems to be a combination of two main effects - groups of well connected fibers are held back or pulled along depending on whether their connections to the left or right edge are stiffer (apparent at the lower right and lower left of the middle figure); and there are swirls where the fibers on opposite sides of open areas are pulled more or less severely (apparent near the upper right corner of the top figure and also at several spots in the bottom figure). To quantitatively describe the non-uniformity in the displacement fields we calculate the root-mean-square (*rms*) difference between each node's actual displacement and what it would be if displacements were uniform. The average *rms* displacement difference for sets of ten networks is 1.66 for floc parameter $b = 0.2$, 2.61 for $b = 1.6$, and 2.86 for $b = 2.4$. While the absolute magnitudes of these numbers are not worth discussing, they clearly show a trend toward less uniformity in the displacement fields as the network geometry becomes less homogeneous.

6. Scale Dependence of Constitutive Laws of Disordered Fiber Networks

Given a disordered network of fibers, such as the ones shown in Figure 4, we are faced with a problem of dependence of effective properties on scale and boundary conditions. A guidance in this respect is provided by the in-plane thermal conductivity of such networks. To this end, we

consider responses of fiber networks under two types of uniform boundary conditions:

(a) Essential:

$$T = T^0_{,j} x_j \tag{21}$$

which yield a conductivity tensor $\boldsymbol{K}^e_\delta$ ('e' stands for essential boundary conditions); here T is the temperature; $T^0_{,j}$ is the spatial average temperature gradient; and x_j is a position vector.

(b) Natural:

$$q = q^0_j n_j \tag{22}$$

which yield a resistivity tensor $\boldsymbol{R}^n_\delta$ ('n' stands for natural boundary conditions); here q is the heat flux on the boundary, q^0_j is the spatial average heat flux vector, and n_j is the outer unit normal to the window's boundary. In the above, we employ boldface for a second-rank tensor and, consistent with (1.2), an overbar for a spatial average over the window domain.

It is useful to note here a 'semi-analogy' - not really a one-to-one correspondence because of different tensor ranks - between the in-plane conductivity and the in-plane elasticity of fiber networks. Moreover, our fiber network, involves micropolar effects, which have no analogy in the thermal conductivity problem. We have:

Table 1:

thermal conductivity	elasticity
temperature T	displacement u_i
temperature gradient T_i	strain ε_{ij}
heat flux through a boundary q	traction at a boundary t_i
heat flux q_i	Cauchy stress σ_{ij}
conductivity K_{ij}	stiffness C_{ijkl}
resistivity R_{ij}	compliance S_{ijkl}

To compute constitutive responses we employ a computer program treating the network as a two-phase material made of conducting fibers (of property K^{fiber}) and poorly conducting pores (of property K^{void}). We work under the following assumptions:

(i) Convection phenomena in the pores are disregarded; this is justified by a consideration of the Grashoff number that is estimated to be definitely less than 1000.

(ii) Radiation phenomena are disregarded since they have a weak contribution to overall conduction compared to the contribution of conduction through the solid fibers; this is true for a network viewed as a cellular solid of density much higher than 10% [24].

(iii) Fiber-fiber bonds present no hindrance to the conductivity, so that the entire network could be regarded as a randomly connected two-phase medium comprising fibers of property K^{fiber} and pores of property K^{void}.

For any realization $B_\delta(\omega)$, a window's response on the mesoscale (δ finite) is, under these definitions, nonunique - because the conductivity $\boldsymbol{K}^e_\delta(\omega)$ is not an inverse of the resistivity $\boldsymbol{R}^n_\delta(\omega)$ almost surely (i.e., with probability one). In fact, $[\boldsymbol{R}^n_\delta(\omega)]^{-1} \leq \boldsymbol{K}^e_\delta(\omega)$, $\forall\delta, \omega$, which can be proven for this case as in case of elasticity [25].

It follows from variational principles, in the context of statistically homogeneous fiber networks, that the effective macroscopic conductivity tensor $\boldsymbol{K}^{eff}$ is bounded by two tensors $\langle \boldsymbol{K}^e_\delta \rangle$ and $\langle \boldsymbol{R}^n_\delta \rangle^{-1}$. Both ensemble averages, indicated by $\langle\ \rangle$, bound the effective conductivity the more the scale $\delta = L/\langle l \rangle$ approaches its continuum limit $\delta \to \infty$, where $\langle l \rangle$ is the average fiber length. Thus, the hierarchy of δ-dependent bounds on $\boldsymbol{K}^{eff}$ applies [21, 22, 25]

$$\langle \boldsymbol{R}^n_{\delta'} \rangle^{-1} \leq \langle \boldsymbol{R}^n_\delta \rangle^{-1} \leq \boldsymbol{K}^{eff} \leq \langle \boldsymbol{K}^e_\delta \rangle \leq \langle \boldsymbol{K}^e_{\delta'} \rangle \qquad \forall\delta' = \delta/2 \tag{23}$$

The order relation employed here is to be understood as follows: for two second-rank tensors $\boldsymbol{A}$ and $\boldsymbol{B}$, $\boldsymbol{B} \leq \boldsymbol{A}$ means that $t \cdot \boldsymbol{B} \cdot t \leq t \cdot \boldsymbol{A} \cdot t$ for any vector $t \neq 0$. In fact, the hierarchy (22) has always been observed in computational mechanics studies for arbitrary $\delta' < \delta$, and this has recently been justified by scaling arguments [27].

This formulation is consistent with the RVE concept [21, 25, 26] according to which the relations between volume average heat flux and temperature gradient should be the same regardless of whether natural or essential boundary conditions have been used; this happens as the sample becomes infinite. In the case of elasticity, a corresponding hierarchy of δ-dependent bounds on the macroscopic, effective stiffness tensor $\boldsymbol{C}^{eff}$ is

$$\langle \boldsymbol{S}_{\delta}^{n} \rangle^{-1} \leq \langle \boldsymbol{S}_{\delta}^{n} \rangle^{-1} \leq \boldsymbol{C}^{eff} \leq \langle \boldsymbol{C}_{\delta}^{e} \rangle \leq \langle \boldsymbol{C}_{\delta'}^{e} \rangle \qquad \forall \delta' = \delta/2 \tag{24}$$

The upper (lower) part of this hierarchy results from uniform kinematic (traction) condition.

Let us now consider a specific example where $K^{void} = 10^{-3} K^{fiber}$ and where fibers' centers are generated according to a hard-core point process with one fiber per germ point, and with fiber lengths following a uniform distribution according to the rule: $l = \langle l \rangle (1 + r)$, with a random number $r \in [-0.5, 0.5]$ and $\langle l \rangle = 1.2mm$; fiber widths are $0.03mm$; see Figure 16(a) of [22]. Fiber orientations follow the angular distribution function (5) with $a_1 = 1$, with all the other terms being zero, so that the network will display the anisotropy.

The hierarchy (23) is illustrated in Figure 5 for window sizes δ up to ten times larger than the fiber length. It is seen that the medium's response based on the estimates $\langle K_{11}^{e} \rangle$ and $\langle K_{22}^{e} \rangle$ resulting from the uniform essential boundary condition (21) levels off much more quickly than that described by $\langle R_{11}^{n} \rangle^{-1}$ and $\langle R_{22}^{n} \rangle^{-1}$ resulting from the uniform natural boundary condition (22). This is also the case at moderate mismatches such as $K^{void} = 0.2 K^{fiber}$, whereby the approach

to RVE is certainly more rapid [22].

Figure 6 displays the plots of boundary data in the essential and natural boundary value problems on the fiber network. Thus (a) gives the case of high contrast, while (b) that of low. In each case, the first plot shows the resulting heat flux $q_1(x_2)$ on the left boundary under (21) with $T^0_{,1} =$ *const*; the second plot shows the resulting temperature distribution $T(x_2)$ under (22) $q^0_1 = \bar{q}_1$ computed from the average of $q_1(x_2)$ in the first problem. In (b) plots of fluxes need to be scaled down by a factor 10 to fit the graph onto the page. This figure indicates that, for low as well as high contrasts, the fluctuations in flux under essential condition are on the same order as the fluctuations in temperature under the natural condition; given the linearity of the problem, we could equivalently run the essential conditions (21) at $T^0 = \bar{T}$ computed from the average temperature $T(x_2)$ of the natural conditions problem.

While there is no one-to-one analogy between the in-plane conductivity and the in-plane elasticity, this study indicates that the essential, rather than natural, boundary conditions lead to relatively scale-independent effective constitutive responses. Roughly speaking, paper may be considered to be a porous plate in which, due to the connectivity of fibers, the temperature gradient (or strain in case of elasticity) is more uniform that the heat flux distribution (or stress in case of elasticity). The situation is opposite in a material reinforced with stiff inclusions. Thus, it is preferable to work with kinematic boundary conditions. In principle, the lower part of the hierarchy (24) can also be computed after adopting a specific, albeit nonunique [28], rule for application of traction boundary condition to a disordered distribution of beams crossing the boundary. Finally, since the frame of fiber-beams cannot undergo affine displacements, a Voigt-type bound is untenable and unattainable. Similarly, a Reuss-type bound is infeasible.

7. Summary

The literature does not unambiguously answer the question of whether or not "special orthotropy" as proposed by Campbell is common in all types of paper. In the present work we consider under what conditions special orthotropy could occur. The Cox model, with its neglect of fiber bending stiffness, can only produce special orthotropy with a few specific fiber orientation distributions. On the other hand, closed form solutions for the effective compliances of a periodic network were used to show that such a network, if anisotropic, cannot satisfy the required conditions. Given the need to consider disordered networks, an analysis of random networks which may contain flocs and other non-homogeneities was used.

Our random fiber network analysis showed that random geometry involving two scales - random fiber placement and orientation as well as flocculation modeled by the germ-grain process - may lead to a macroscopic property of special elastic orthotropy. This result is dependent on taking into account the flexural and shear deformation of fibers in addition to their axial deformation. The evaluation of parameter space was not comprehensive, so there likely are other combinations of parameters to achieve the same relation among the effective material properties. Such potentially important parameters as fiber curl, ratio of fiber flexibility to bond flexibility, and ratio of fiber flexural stiffness to fiber axial stiffness were not evaluated.

A demonstration was made regarding the non-uniformity of the displacement fields in these networks. It was shown that decreasing the degree of geometric homogeneity decreases the uniformity of the displacement field. Non-uniformity of the displacement field is likely to have a significant effect on the progression of microfailures that leads to a network's stiffness degradation and failure. Fiber and/or bond failures are likely to occur in areas of relatively intense deformation before they would occur if the deformation were uniform. Consequently,

network effective strengths should be lower than they would be if the strain were uniform. This is the subject of continuing work.

Finally, in Section 6, we considered the issue of scale dependence of effective properties. A guidance in this respect is provided by the in-plane thermal conductivity of fiber networks under two types of boundary conditions: essential and natural. This study indicates that the essential boundary conditions lead, more rapidly than the natural ones, to relatively scale-independent effective constitutive responses.

Acknowledgment

Support of this research by the IPST member companies, the National Science Foundation under grant CMS-9713764, and Milwaukee School of Engineering is gratefully acknowledged. We appreciate the comments of referees.

Bibliography

[1] C.C. Habeger, *Personal communication*, Institute of Paper Science and Technology (1997).

[2] M. Horio and S. Onogi, Dynamic measurements of physical properties of pulp and paper by audiofrequency sound, *J. Appl. Phys.* **22** (1951) 971-977.

[3] J.G. Campbell, The in-plane elastic constants of paper, *Austral. J. Appl. Sci.* **12** (1961) 356-357.

[4] J.K. Craven and D.L. Taylor, Nondestructive sonic measurement of paper elasticity, *TAPPI J.* **48**(3) (1965) 142-147.

[5] A.R. Jones, An experimental investigation of the in-plane elastic moduli of paper, *TAPPI J.* **51**(5) (1968) 203-209.

[6] J.C. Suhling, M.W. Johnson, R.E. Rowlands and D.E. Gunderson, Nonlinear elastic constitutive relations for cellulosic materials, *Mechanics of Cellulosic and Polymeric Materials*. In R.W. Perkins (ed.), ASME **AMD-99**, 1-13 (1989).

[7] J.Y. Liu and R.J. Ross, Shear modulus variation with grain slope, *Mechanics of Cellulosic Materials*. In R.W. Perkins (ed.), ASME **AMD-221/MD-77**, 107-112 (1997).

[8] K. Schulgasser, On the in-plane elastic constants of paper, *Fiber Sci. Tech.* **15**, 257-270 (1981).

[9] H.L. Cox, The elasticity and strength of paper and other fibrous materials, *Brit. J. Appl. Phys.* **3** (1952) 72-79.

[10] K. Schulgasser and D.H. Page, The influence of transverse fibre properties on the in-plane elastic behaviour of paper, *Compos. Sci. Tech.* **32** (1988) 279-292.

[11] M. Ostoja-Starzewski and D.C. Stahl, Random fiber networks and special orthotropic elasticity of paper, *Mechanics of Cellulosic Materials*. In R.W. Perkins (ed.), ASME **AMD-231/MD-85** (1999) 23-29.

[12] D.H. Page, P.A. Tydeman and M. Hunt, A study of fibre-to-fibre bonding by direct observation, *The Formation and Structure of Paper - Trans. Oxford Symposium* **1** (1961) 171-19.

[13] M. Ostoja-Starzewski, M.B. Quadrelli and D.C. Stahl, Kinematics and stress transfer in quasi-planar random fiber networks, *C. R. Acad. Sci. Paris IIb*, **327**, 1223-1229 (1999).

[14] C. Wozniak, *Surface Lattice Structures* (in Polish), Polish Sci. Publishers, Warsaw (1970).

[15] W. Nowacki, *Theory of Asymmetric Elasticity*, Oxford, Pergamon Press/Polish Scientific Publishers/Warsaw (1986).

[16] I. Jasiuk and M. Ostoja-Starzewski (eds.), *Micromechanics of Random Media II* - Spec. Issue

of *Intl. J. Solids Struct.* **35**(19) (1998).

[17] D. Stoyan, W.S. Kendall and J. Mecke, *Stochastic Geometry and its Applications*, John Wiley & Sons, New York (1987).

[18] M. Deng and C.T.J. Dodson, *Paper: an Engineered Stochastic Structure*, TAPPI Press, Atlanta (1994).

[19] D.C. Stahl and S.M. Cramer, A three-dimensional network model for a low density fibrous composite, *ASME J. Engng. Mat. Tech.* **120**(2) (1998) 126-130.

[20] D.C. Stahl and E.P. Saliklis, A non-homogeneous network model for paper. In R.W. Perkins (ed.), *Mechanics of Cellulosic Materials*, ASME **AMD-221/MD-77**, 19-25 (1997).

[21] R. Hill, Elastic properties of reinforced solids: some theoretical principles. *J. Mech. Phys. Solids* **11** (1963) 357-372.

[22] M. Ostoja-Starzewski, Random field models of heterogeneous materials, *Intl. J. Solids Struct.* **35**(19) (1998) 2429-2455.

[23] K. Ding and G.J. Weng, The influence of moduli slope of a linearly graded matrix on the bulk moduli of some particle- and fiber-reinforced composites, *J. Elast.* **53** (1999) 1-22.

[24] L.J. Gibson and M.F. Ashby, *Cellular Solids*, Pergamon Press, Oxford (1988).

[25] C. Huet, Application of variational concepts to size effects in elastic heterogeneous bodies, *J. Mech. Phys. Solids* **38** (1990), 813-841.

[26] M. Ostoja-Starzewski and J. Schulte, Bounding of effective thermal conductivities of multiscale materials by essential and natural boundary conditions, *Phys. Rev. B* **54** (1996), 278-285.

[27] M. Ostoja-Starzewski, Scale effects in materials with random distributions of needles and cracks, *Mech. Mater.* **31**(12), 883-893 (1999).

[28] M. Ostoja-Starzewski and C. Wang, Linear elasticity of planar Delaunay networks. II: Voigt and Reuss bounds, and modification for centroids, *Acta Mech.* **84** (1990), 47-61.

[29] D. Jeulin and M. Ostoja-Starzewski, Eds., *Mechanics of Random and Multiscale Microstructures*, CISM Lecture Notes, Springer-Verlag, to appear (2000/01).

Figure Legends

Figure 1. A perspective view of a triangular, periodic fiber-beam network.

Figure 2. Network effective modulus from present analysis compared to the Cox model, as affected by sheet thickness t (*RBA* decreases as t increases) and flocculation parameter b (flocs tighten as b increases).

Figure 3. Relation of the Campbell number to sheet thickness t (RBA decreases as t increases), flocculation parameter b, and fiber orientation function of equation (5).

Figure 4. Undeformed network geometry (on the left) and differences of true node displacements from those that would result under an affine displacement field due to overall uniform strain $\varepsilon_{ij}^{0} = const$ (on the right).

Figure 5. Hierarchies of bounds, normalized by K^{fiber}, for random fiber systems, showing convergence of $\langle K_{11}^{e} \rangle$ and $\langle R_{11}^{n} \rangle^{-1}$ as well as $\langle K_{22}^{e} \rangle$ and $\langle R_{22}^{n} \rangle^{-1}$ with increasing mesoscale δ; $K^{void} = 10^{-3}$.

Fig. 6. Thermal responses of a finite fiber systems with (a) $K^{void} = 10^{-3} K^{fiber}$ and (b) $K^{void} = 0.2K^{fiber}$, both at 40% porosity. In each case, the first figure shows the resulting $q_1(x_2)$ on the left and right boundaries under uniform essential b.c.'s (21) $T_{,1}^{0} = const$, while the second one shows response $T(x_2)$ under uniform natural b.c. (22) $q_1^{0} = const$ computed from the volume averages of $q_1(x_2)$ in the first problem. In (b) plots of fluxes are scaled down by a factor 10.

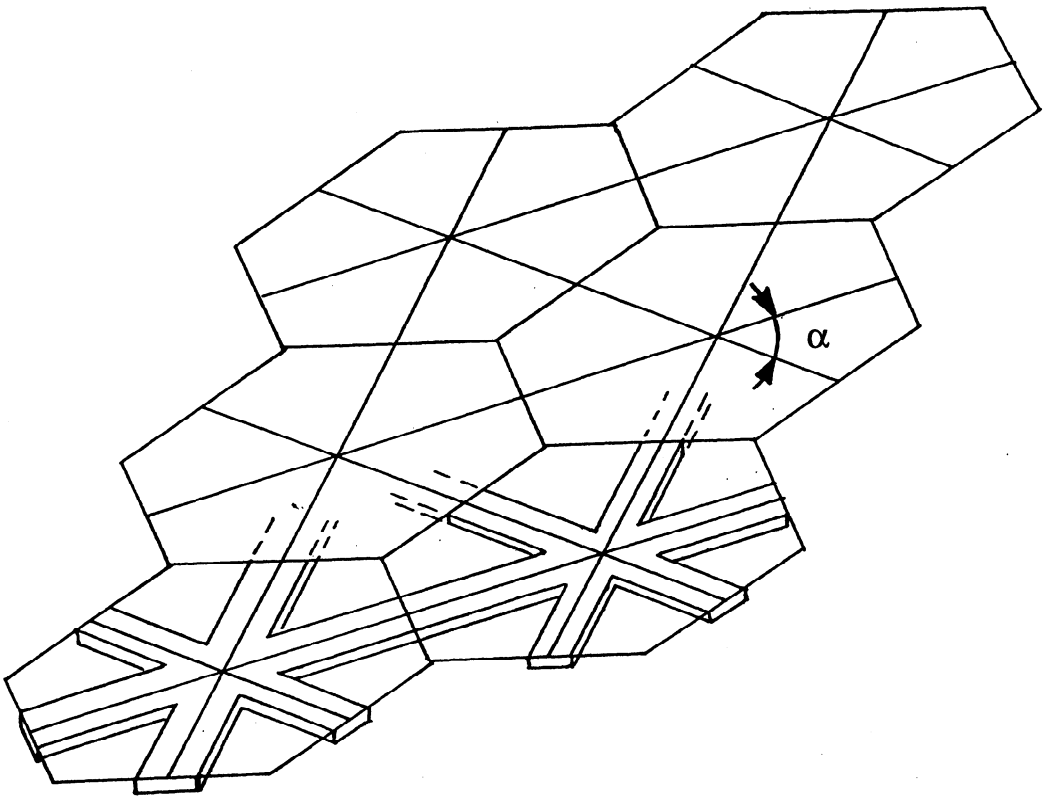

Figure 1

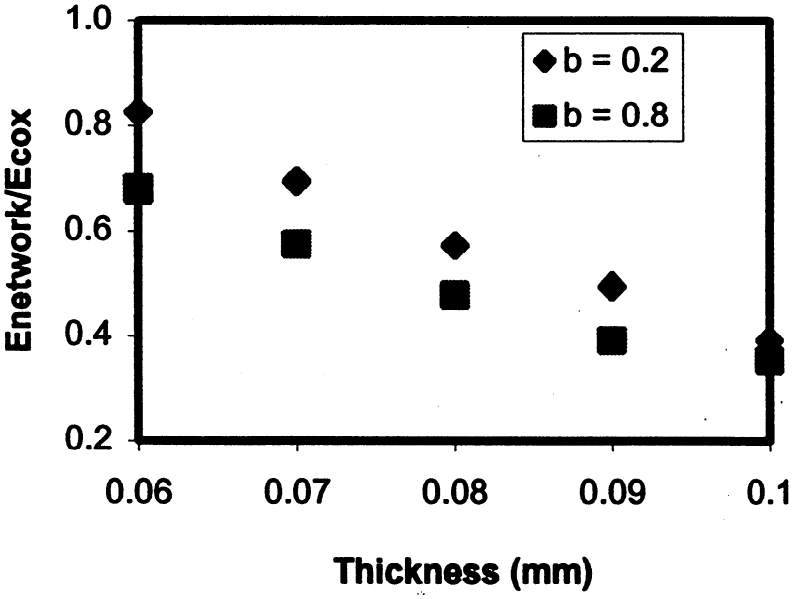
1.0
0.8
0.6
0.4
0.2
Enetwork/Ecox
b = 0.2
b = 0.8
0.06
0.07
0.08
0.09
0.1
Thickness (mm)

Figure 2

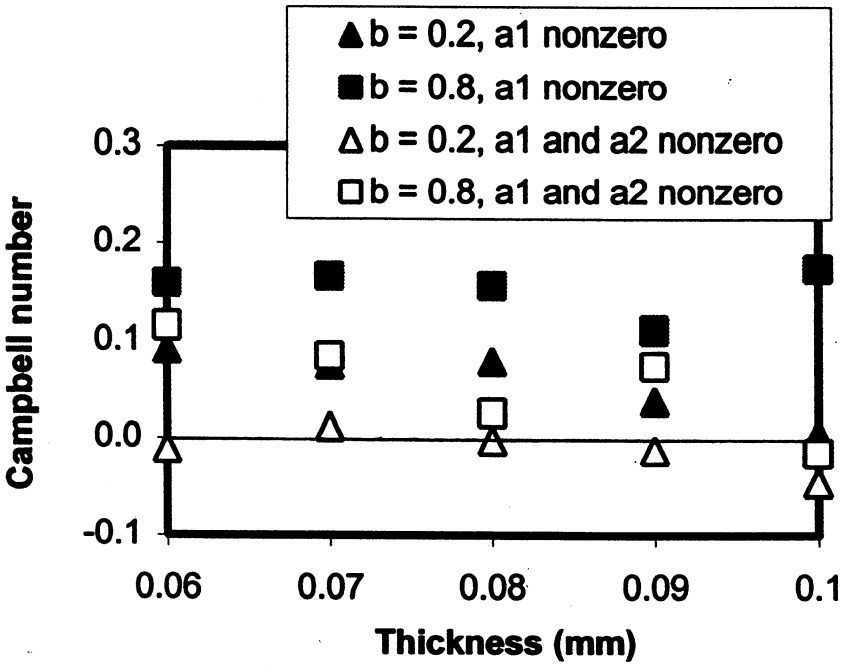
b = 0.2, a1 nonzero
b = 0.8, a1 nonzero
b = 0.2, a1 and a2 nonzero
b = 0.8, a1 and a2 nonzero
Campbell number
0.3
0.2
0.1
0.0
-0.1
0.06
0.07
0.08
0.09
0.1
Thickness (mm)

Figure 3

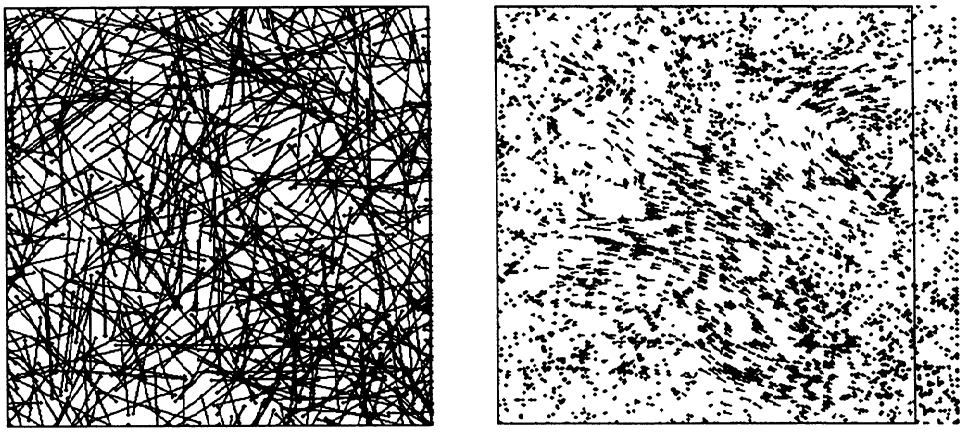

a) floc parameter b = 0.2

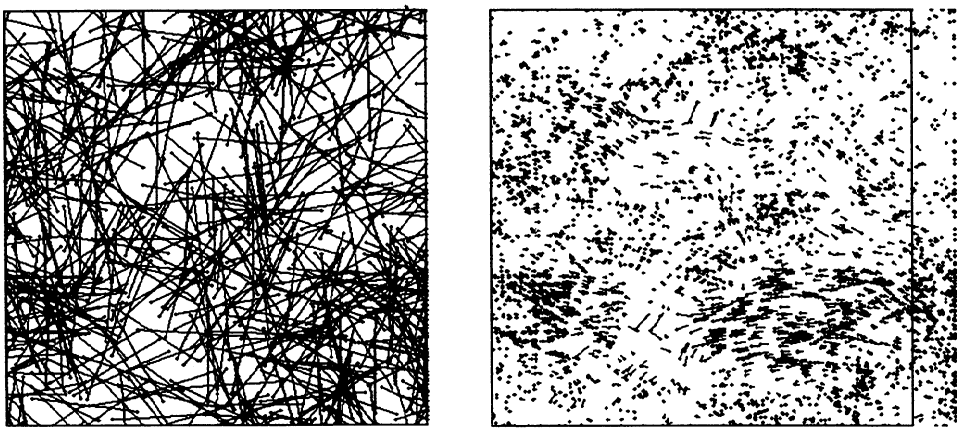

b) floc parameter b = 1.6

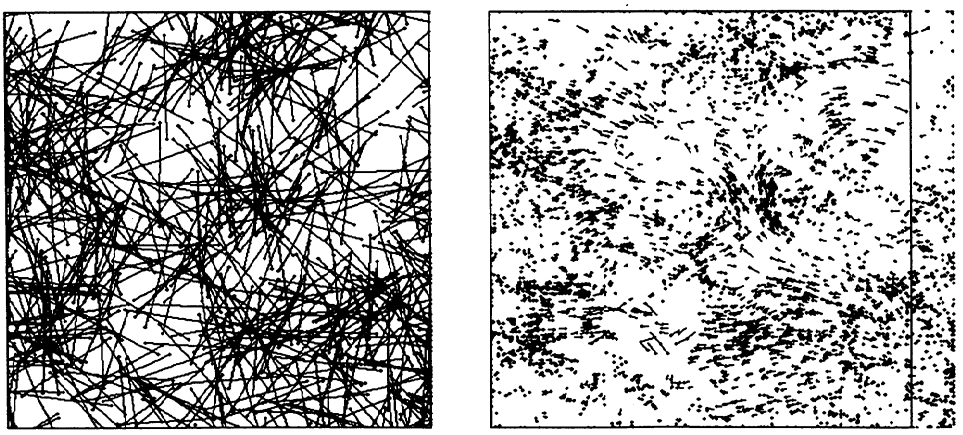

c) floc parameter b = 2.4

Figure 4

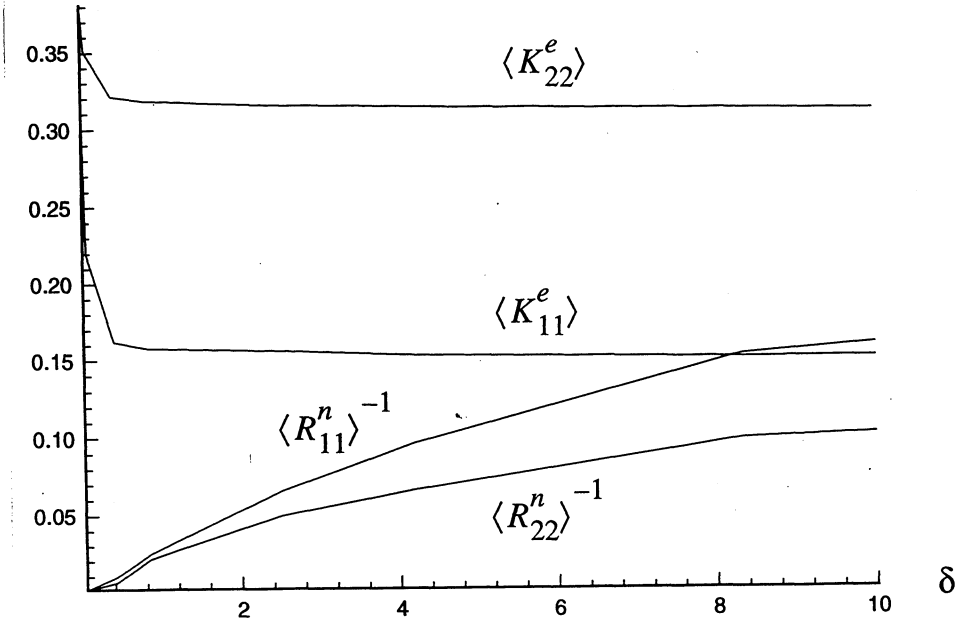
0.35
0.30
0.25
0.20
0.15
0.10
0.05
2
4
6
8
10
$\langle K_{22}^e \rangle$
$\langle K_{11}^e \rangle$
$\langle R_{11}^n \rangle^{-1}$
$\langle R_{22}^n \rangle^{-1}$
δ

Figure 5

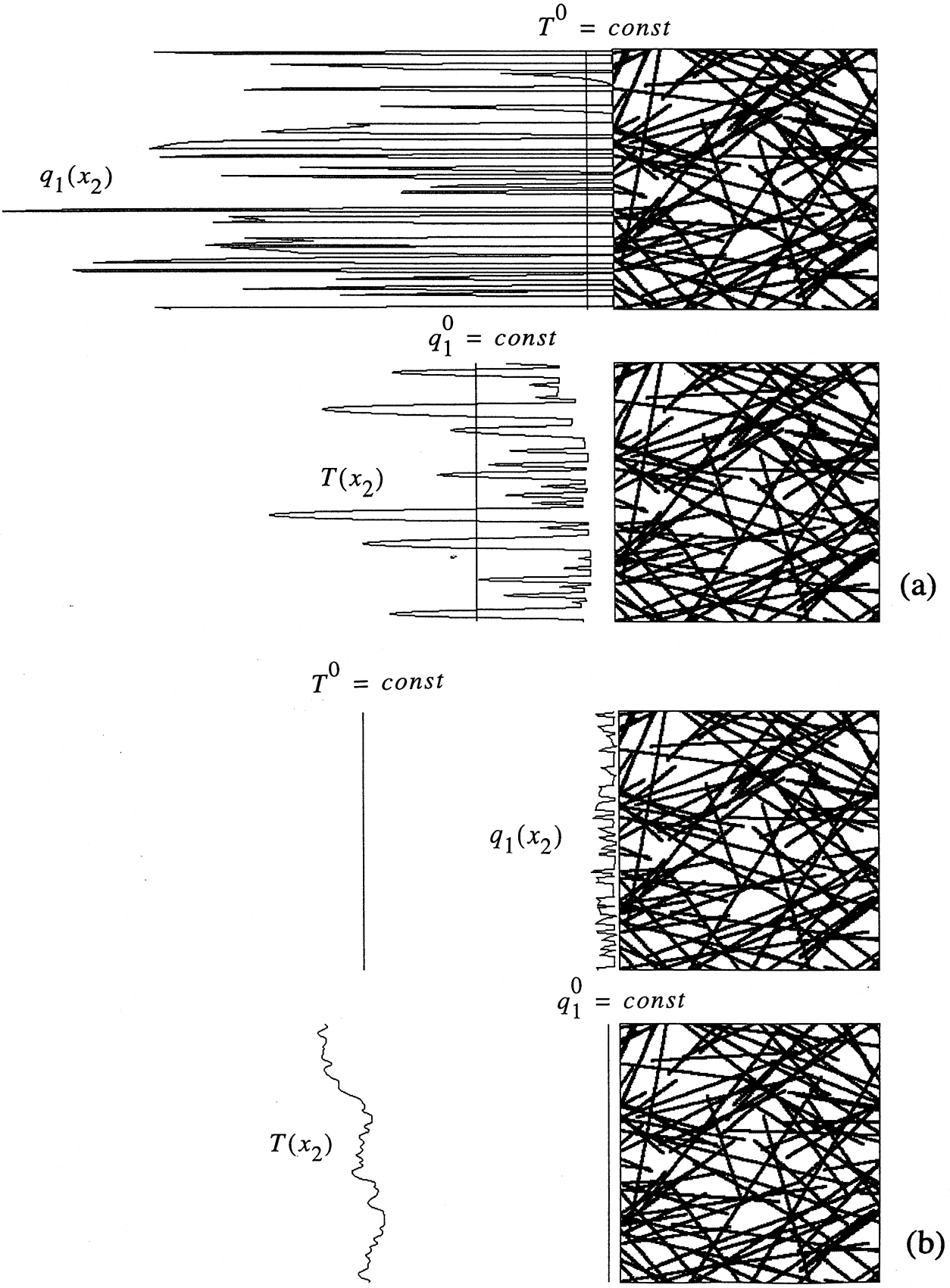

Figure 6